RESEARCH ARTICLE

Biosorption of Cr(III) and Pb(II) from synthetic wastewater under dynamic conditions – diffusion characteristics

P.A. Kotabewatta, Linda B.L. Lim and N. Priyantha*

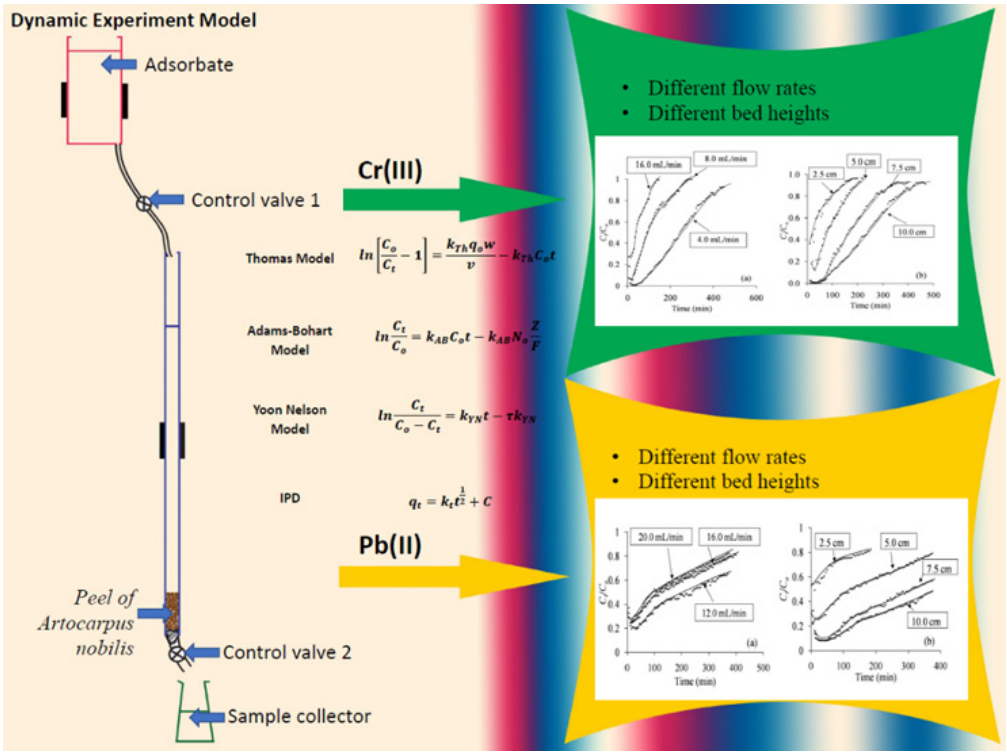

Highlights

- Cr(III) or Pb(II) can be removed under dynamic conditions using the biosorption technique developed.
- Intra-particle diffusion (IPD) model can be applied for dynamic process of heavy metal removal.
- Boundary layer thickness (barrier) developed by adsorbate on biosorbent can be controlled by changing flow rate and bed height of the dynamic adsorption system.

Ceylon Journal of Science 52 (1) 2023: 71-81
DOI: http://doi.org/10.4038/cjs.v52i1.8106

RESEARCH ARTICLE

Biosorption of Cr(III) and Pb(II) from synthetic wastewater under dynamic conditions – diffusion characteristics

P.A. Kotabewatta[1,2], Linda B.L. Lim[3] and N. Priyantha[2,4,*]

[1]*Postgraduate Institute of Science, University of Peradeniya, Peradeniya, Sri Lanka*
[2]*Department of Chemistry, University of Peradeniya, Peradeniya, Sri Lanka*
[3]*Department of Chemistry, University of Brunei Darussalam, Gadong BE1410, Brunei Darussalam*
[4]*Institute of Chemistry Ceylon, Adamantane House, 341/22 Kotte Road, Rajagiriya, Sri Lanka*

Received: 22.11.2021; Accepted: 15.01.2023

Abstract: Investigation of diffusion characteristics of adsorption systems under dynamic conditions has not received much attention despite its necessity of extending findings of static systems toward real-time applications. A biosorption system consisting of peel ($710 < d < 1000$ µm) of the fruit of *Artocarpus nobilis* biosorbent and Cr(III) or Pb(II) adsorbate shows that the rate constant evaluated according to the Thomas model (k_{Th}), saturation concentration (N_o) of the Adams-Bohart model and the rate constant of the Yoon Nelson model (k_{YN}) show a direct relationship with the flow rate and an inverse relationship with equilibrium uptake per unit mass of adsorbent (q_o). The opposite trend is observed with increase in bed height. The Weber and Morris intra-particle diffusion model shows that the boundary layer thickness (C) of the biosorbent depends on both the flow rate and the bed height. On the other hand, the intercept of the linear relationship between the extent of adsorption q_t vs. $t^{1/2}$ (contact time) decreases with increase in bed height for both Cr(III) and Pb(II). The special feature of the negative intercepts observed in this dynamic biosorption system is indicative of retardation of intra-particle diffusion of Cr(III) and Pb(II) toward the biosorbent. The next logical step of this research would be the extension of this research in prototype systems.

Keywords: Adams–Bohart model, *Artocarpus nobilis*, Intraparticle diffusion (IPD) model, Thomas model, Yoon Nelson model

INTRODUCTION

Biosorption provides efficient means to decrease levels of heavy metal ions in the aquatic environment (Albadarin *et al*., 2011; Yan *et al*., 2010). Adsorption isotherm models, namely, Langmuir, Freundlich, Tempkin and Redlich-Peterson, have been applied to biosorption systems in an attempt to understand the metal ion-biosorbent interactions (Chieng *et al*., 2015; Lim *et al*., 2015; Priyantha *et al*., 2018). Although maximum adsorption capacity and isotherm constants have been estimated through the above models, application of biosorption methods for large-scale removal of metal ions in industrial setting is still at an infant stage.

Removal of metal ions in industrial scale is usually performed in dynamic reactors. Owing to the continuous flow of solutions containing metal ions, such systems do not reach equilibrium state, and hence, adsorption models designated for batch experiments cannot be directly applied for dynamic systems. In this context, dynamic adsorption models have been formulated by modifying static adsorption models. Consequently, some adsorption models have been applied for metal ion removal studies under dynamic conditions (Lim and Aris, 2014; Xu *et al*., 2013). Nevertheless, neither extrapolation of the above models toward real applications with larger volumes nor comparison among various parameters determined from each model has been well documented.

The Thomas Model does not consider axial dispersion in describing adsorption-desorption rates. This model leads to the estimation of adsorption capacities, and assumes second-order reversible reaction kinetics (Yan *et al*., 2010; Gutiérrez-Segura *et al*., 2014). On the other hand, the Adams-Bohart Model considers that the sorption equilibrium is not instantaneous, and that the rate of sorption is proportional to the remaining fraction of sorption sites on the sorbent. A special feature of this model is that it focuses on the early stage of the adsorption breakthrough curve (Han *et al*., 2009; Zheng *et al*., 2016). A major assumption of the Yoon Nelson Model is that the rate of decrease in the probability of adsorption of adsorbate species is positively correlated to the probabilities of both adsorption and breakthrough of the adsorbate (Chatterjee *et al*., 2018; Aksu and Gönen, 2004). The linearized relationships of the above three models are given in Table 1.

Lead removal experiments using biosorbents, such as *Agaricus bisporus*, water hyacinth root and rubber wood sawdust, have been reported in literature. However, the parameters of Thomas, Adams-Bohart and Yoon Nelson models depend on the type of sorbent and the conditions applied (Long *et al*., 2014; Mitra *et al*., 2014; Biswas and

**Corresponding Author's Email: namalpriyantha@sci.pdn.ac.lk*
https://orcid.org/0000-0001-8625-8579

Table 1: Linearized relationships of dynamic models.

Model	Equation	Reference
Thomas Model	$ln\left[\frac{C_o}{C_t}-1\right]=\frac{k_{Th}q_o w}{v}-k_{Th}C_o t$	(Hasan *et al*., 2010; Saadi *et al*., 2013)
Adams-Bohart Model	$ln\frac{C_t}{C_o}=k_{AB}C_o t-k_{AB}N_o\frac{Z}{F}$	(Lim & Aris, 2014; Wang *et al*., 2015)
Yoon Nelson Model	$ln\frac{C_t}{C_o-C_t}=k_{YN}t-\tau k_{YN}$	(Foo & Hameed, 2010; (Malkoc *et al*., 2006)

Note: k_{Th} ($mLmin^{-1}\ mg^{-1}$) = Thomas rate constant; q_o (mgg^{-1}) = Equilibrium uptake per gram of adsorbent; C_o (mgL^{-1}) = Influent metal ion concentration; C_t (mgL^{-1}) = Effluent concentration at time t; w (g) = Mass of adsorbent; v ($mLmin^{-1}$) = Flow rate; k_{AB} ($Lmg^{-1}\ min^{-1}$) = Kinetic constant; F (cmmin-1) = Linear velocity; Z (cm) = Bed depth of column; N_o (mgL^{-1}) = Saturation concentration; k_{YN} (min^{-1}) = Yoon Nelson rate constant; τ (min) = Time required for 50% adsorbate breakthrough.

Mishra, 2015). Similar observation has been reported for chromium removal experiments as well (Kumar *et al*., 2020).

Weber and Morris described the intra-particle diffusion (IPD) model, which helps to determine the rate constant and the boundary layer resistance, thereby describing the intra-particle diffusion taking place during adsorption (Gerente *et al*., 2007; Santhi and Manonmani, 2011). The initial relationship of the IPD model for batch-adsorption studies is $q_t = k_t t^{1/2}$, where q_t (mg g^{-1}) is the extent of adsorption when time = t and k_t [mg g^{-1} $min^{-1/2}$] is the IPD rate constant. As many adsorption systems do not follow the above relationship with regard to the zero intercept, a modified version to include a non-zero intercept (C) is proposed (Lim *et al*., 2013; Ofomaja, 2010), as given by,

$$q_t = k_t t^{\frac{1}{2}} + C \quad (1)$$

The intercept of the above relationship is directly related to the extent of the boundary layer thickness, where higher values of the intercept lead to enhanced boundary layer effect influenced by experimental parameters, such as contact time and rate of adsorption (Ofomaja, 2010; Ali *et al*., 2016; Sheela and Nayaka, 2012; Zhou *et al*., 2011). Consequently, the intercept depends on the particle size, surface area of the adsorbent and the concentration of the external solution (Ali *et al*., 2016; Aljeboree *et al*., 2017; Özcan and Özcan, 2004). Some IPD plots have shown multi-linearity in the biosorption process as per Equation (1) above, where three linear portions have been identified: the first portion is the external mass transfer process; the second one is related to the rate limiting step of diffusion; and the last step indicates adsorption which decreases with time. Adsorption behaviour of the biosorbent-adsorbete system at initial stage is described by the initial adsorption factor (R_i), represented in Equations 2 and 3 obtained by rearranging the IPD model (Mckay, 2007; Ting *et al*., 2016; Wu *et al*., 2009).

$$\left(\frac{q_t}{q_{ref}}\right) = 1 - R_i\left[1-\left(\frac{t}{t_{ref}}\right)^{1/2}\right] \quad (2)$$

and,

$$R_i = \frac{q_{ref}-C_i}{q_{ref}} = 1-\left(\frac{C_i}{q_{ref}}\right) \quad (3)$$

where t_{ref} is the longest time in the adsorption process and q_{ref} is the solid phase concentration of the adsorbate at $t = t_{ref}$ and C_i is the initial concentration of the adsorbate.

In addition to intra-particle diffusion, many steps of mass transfer would occur during biosorption in dynamic systems. These include liquid phase mass transfer, molecular diffusion, interface diffusion (film diffusion), mass transport from mobile phase to stationary phase, adsorption-desorption and intra-particle diffusion (Xu *et al*., 2013; Crittenden *et al*., 1986; Girish and Murty, 2016). Therefore, biosorption which is a complicated process becomes even more complex in dynamic systems. Detailed investigation of the applicability of diffusion models to dynamic systems has not been paid much attention, probably due to their complexity, despite the necessity of understanding mass transfer processes.

In this context, dynamic models, namely, the Adams-Bohart Model, the Thomas Model, and the Yoon Nelson Model were applied for a biosorption system under dynamic conditions, which involves Cr(III) and Pb(II) adsorbates present in synthetic solutions, and peel of *Artocarpus nobilis* fruit as the biosorbent. Breadfruit (*Artocarpus sp*.) consist of about fifty varieties most of which are rich in phenolic compounds, such as, flavonoids, stilbenoids, arylbenzofurons, and carboxylic acids and their derivatives. These functional groups form negative ions in aqueous medium, thereby showing affinity toward heavy metal ions (Jagtap and Bapat, 2010; Al-Asheh *et al*., 2000). Further, these functional groups, together with the high porosity of the biosorbent lead to increase removal ability of heavy metal ions through biosorption (Priyantha and Kotabewatta, 2019). The *Artocarpus nobilis* plant is endemic to Sri Lanka, and not much attention has been paid as a biosorbent, and hence, the peel of *Artocarpus nobilis* fruit was investigated for its removal ability toward heavy metal ions, namely Cd(II) and Pb(II). The surface morphology and the elemental composition of the raw biosorbent examined using scanning electron microscopy (SEM) and energy-dispersive X-ray spectroscopy (EDX) reveal the inhomogeneity of the biosorbent surface, and

the presence of K and Ca (Kotabewatta *et al*., 2020). Biosorption generally takes place at the interface of the biosorbent, and diffusion processes take place at biosorbent pores of different sizes, namely micropores, mesopores and macropores. Therefore, external environmental conditions, such as concentration, temperature, pH and agitation speed directly affect biosorption and diffusion processes taking place on the biosorbent. As dynamic systems are open systems which continuously change the adsorbate volume, the concentration gradient may be created along the system, and the diffusion process would change with flow rate and adsorbent bed height. However, adsorption kinetics that takes place on the interface of the biosorbent and in the biosorbent should be approximately the same. Therefore, the application of diffusion models, such as the IPD model for both batch and dynamic biosorption systems should be reasonable. Therefore, an innovative approach was made in this research to apply the modified form of the Weber and Morris intra-particle diffusion model for investigation of biosorption of the above system under dynamic conditions, and to interpret the variation of the nonzero intercepts of the model under different dynamic experimental conditions for the biosorption system.

MATERIALS AND METHODS

Chemicals and reagents

Analytical grade $Cr(NO_3)_3$ and $Pb(NO_3)_2$ were used to prepare standard solutions throughout the study. Stock solutions of 1,000 mg L^{-1} of each compound were prepared and diluted as needed with distilled water.

Preparation of biosorbent

Representative samples of *Artocarpus nobilis* fruits were collected from different locations in the Central Province of Sri Lanka. Peel of matured and ripened fruits was removed, air-dried, separated into desired sizes and kept in dry until characterization and adsorption studies were performed. Particles of diameter $710 < d < 1000$ µm were used as the biosorbent for all column experiments.

Research methodology and instrumentation

Glass tubes (Pyrex) of known internal diameter (1.0 cm) were packed with the biosorbent, and synthetic metal ion solutions of 10.0 mg L^{-1} were introduced to packed columns. Eluent samples of each packed column at different pre-determined flow rates were collected at five-minute time intervals. All spectroscopic measurements were recorded on Spectro-Electronic M Series atomic absorption spectrophotometer, and all experiments were performed at ambient temperature of 27±1 °C in triplicate. The concentrations of Cr(III) and Pb(II) in all solutions were determined using atomic absorption spectrophotometry (AAS) with the aid of freshly constructed calibration curves, and the average values were used for interpretation. A mass of 1.5 g of the biosorbent was required to pack the column up to 5.0 cm bed height.

RESULTS AND DISCUSSION

Dynamic adsorption models

Extents of removal of Cr(III), determined for a column packed up to 10.0 cm within the first 50 min, are 98, 88 and 62% at 4.0, 8.0 and 16.0 mL min^{-1} flow rates, respectively, and a typical breakthrough curve is observed at the slowest flow rate among the three rates [Figure 1(a)]. Such a high extent of removal is expected due to the presence of carboxylic acid groups, phenolic acid groups and their derivatives identified by Fourier transform infrared spectroscopy, and the surface negativity obtained under ambient condition (Priyantha and Kotabewatta, 2019). Further, biosorption of Cr(III) on olive stone indicates that the flow rate at the classic breakthrough curve can be considered as the optimum flow rate for characterization of the adsorption system (Calero *et al*., 2009; Marzbali and Esmaieli, 2017). The breakthrough curves considering the extents of removal of Cr(III) determined at the bed heights of 2.5, 5.0, 7.5 and 10.0 cm at a flow rate of 4.0 mL min^{-1} are shown in Figure 1(b). The removal percentages of Cr(III) within the first 50 min of column operation for at the above bed heights were determined to be 50, 81, 99 and 98%, respectively.

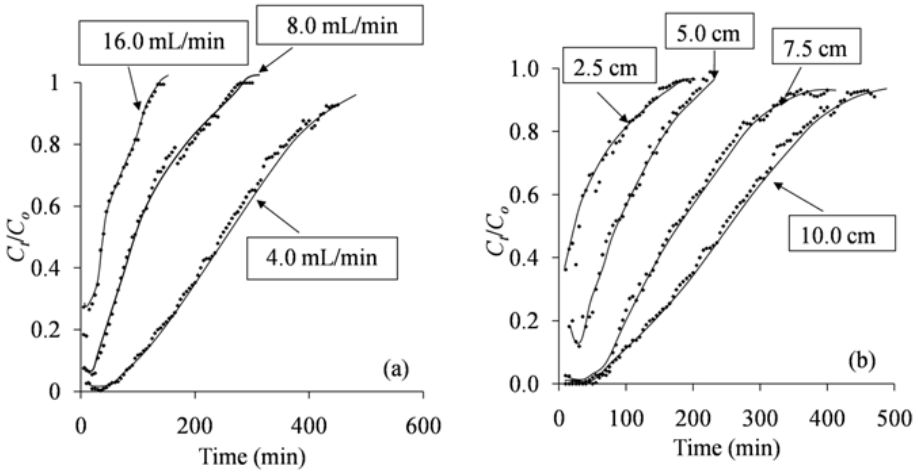

Figure 1: Breakthrough curves of C_t/C_o vs. contact time for interaction of Cr(III) of 10.0 mg L^{-1} concentration with the biosorbent under dynamic condition; (a) At different flow rates for 10.0 cm column packing (b) At different bed heights at a flow rate of 4.0 mL min^{-1}.

Removal percentages of 78, 72 and 70% were shown by Pb(II) solutions at the flow rates of 12.0, 16.0 and 20.0 mL min^{-1} [Figure 2(a)]. Using the same argument of the maximum removal efficiency with high breakthrough time, a flow rate of 16.0 mL min^{-1} was selected as the optimum for investigation of biosorption of Pb(II). Infromation from the breakthrough curves at the above flow rate shown in Figure 2(b) leads to the removal percentages of 42, 72, 90 and 90% at bed heights of 2.5, 5.0, 7.5 and 10.0 cm, respectively. The remaining concentrations of Cr(III) and Pb(II) in each elute at different flow rates and for each bed height, determined by atomic adsorption spectroscopy, when applied to dynamic adsorption models, lead to the results shown in Table 2 and Table 3.

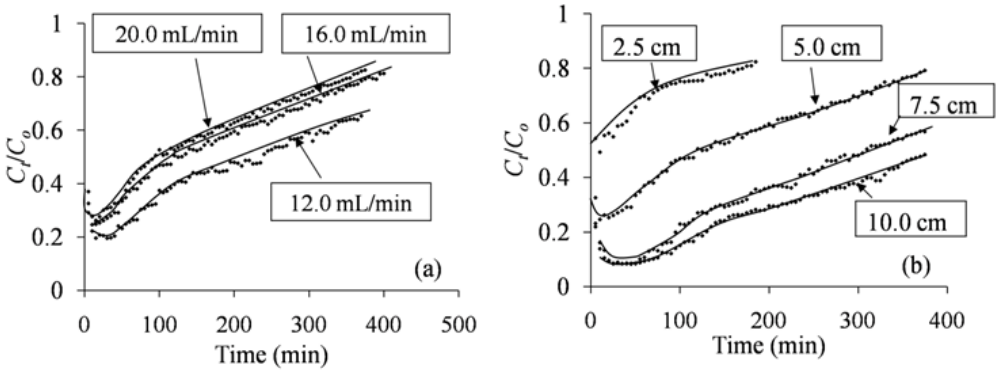

Figure 2: Breakthrough curves of C_t/C_o vs. contact time for interaction of Pb(II) of 10.0 mg L^{-1} concentration with the biosorbent under dynamic condition; (a) At different flow rates for 5.0 cm column packing (b) At different bed heights at a flow rate of 16.0 mL min^{-1}.

Table 2: Parameters of dynamic adsorption models for the interaction of Cr(III) at different flow rates and bed heights.

Flow rate (mL min^{-1})	Thomas Model			Adams – Bohart Model		
	k_{th} (mL mg^{-1} min^{-1})	q_o (mg g^{-1})	R^2	$k_{AB}\times10^{-3}$ (L mg^{-1} min^{-1})	N_o (mg L^{-1})	R^2
4.0	1.44	3.73	0.930	3.50	858	0.964
8.0	1.99	2.88	0.939	2.56	1,157	0.967
16.0	3.63	2.24	0.967	1.40	3,890	0.862
Bed height (cm)						
2.5	2.44	1.27	0.983	1.05	1,871	0.866
5.0	2.63	2.23	0.965	2.04	1,076	0.910
7.5	1.76	2.93	0.925	4.70	895	0.814
10.0	1.34	3.74	0.930	3.64	818	0.964

Flow rate (mL min^{-1})	Yoon Nelson Model			
	$k_{YN}\times10^{-2}$ (min^{-1})	τ (min) (Model)	τ (min) (Experiment)	R^2
4.0	1.57	256	245	0.930
8.0	1.97	109	90	0.930
16.0	3.44	45	40	0.967
Bed height (cm)				
2.5	2.05	28	30	0.983
5.0	2.40	92	80	0.965
7.5	1.52	191	170	0.925
10.0	1.58	251	240	0.930

Table 3: Parameters of dynamic adsorption models for the interaction of Pb(II) at different flow rates and bed heights.

Flow rate (mL min^{-1})	Thomas Model			Adams – Bohart Model		
	k_{th} (mL mg^{-1} min^{-1})	q_o (mg g^{-1})	R^2	$k_{AB}\times10^{-3}$ (L mg^{-1} min^{-1})	N_o (mg L^{-1})	R^2
12.0	0.684	14.93	0.948	0.93	5,912	0.939
16.0	0.773	12.50	0.972	1.02	6,057	0.977
20.0	0.689	12.23	0.980	1.08	7,041	0.973
Bed height (cm)						
2.5	1.564	0.12	0.945	0.52	10,054	0.944
5.0	0.786	12.76	0.975	1.02	6,057	0.977
7.5	0.997	15.43	0.930	1.41	5,484	0.950
10.0	0.772	15.88	0.957	1.16	4,951	0.957

Flow rate (mL min^{-1})	Yoon Nelson Model			
	$k_{YN}\times10^{-3}$ (min^{-1})	τ (min) (Model)	τ (min) (Exp)	R^2
12.0	5.5	232	240	0.948
16.0	6.0	150	130	0.972
20.0	5.5	106	93	0.974
Bed height (cm)				
2.5	7.8	19	10	0.948
5.0	5.9	149	130	0.972
7.5	7.4	301	310	0.934
10.0	6.0	383	380	0.955

Increase in flow rate causes the reduction of retention time leading to inadequate time for biosorption within the column. Therefore, metal ion uptake would decrease, and the rate constant would increase due to higher flow rate. This trend is clearly observed for biosorption of Cr(III) with regard to k_{Th}, q_o and k_{YN} (Table 2). Fixed bed column using waste acorn of *Quercus ithaburensis* for removal of Cr(III) has also shown similar occurrences of the Thomas and Yoon Nelson models (Malkoc *et al*., 2006). Similar trend in the extent of removal (q_o) with no clear trend for k_{th} and k_{YN} was observed for Pb(II) in this study, as shown in Table 3.

Expected trend with the flow rate is not observed in k_{AB} values determined from the Adams-Bohart Model for Cr(III), indicating that this model is not suitable in explaining the biosorption of Cr(III) on the biosorbent. On the other hand, the expected trend in k_{Th} and k_{YN} values are not observed in the Thomas and Yoon Nelson Models for biosorption of Pb(II) although the Adams-Bohart Model leads to the expected trend in k_{AB} values indicating its validity for biosorption of Pb(II) on the biosorbent. In addition, the bed column studies for removal of Pb(II) with nanostructured γ-alumina indicate that the values of k_{Th}, K_{YN} and k_{AB} increase with increase in flow rate and decreased with increase in bed height (Saadi *et al*., 2013). Moreover, similar studies using a synthesized adsorbent removal of Pb(II) has shown that k_{Th} follows the proper trend while q_o deviates (Shahbazi *et al*., 2011). Therefore, the models that are valid could be used in designing treatment systems for each metal in large-scale applications. The experimental value of τ and corresponding model values calculated at different flow rates and bed heights show a good agreement suggesting that τ values obtained from the Yoon Nelson Model be used to obtain information for the construction of bed columns with high heavy metal removal efficiencies. A similar situation for the variations of K_{YN} and τ have been reported by dried straw of *Triticum aestivum* as an effective biosorbent for removal of Cr(III) and Pb(II) at different bed columns (Farooq *et al*., 2013). Further, it is argued that film resistance (thickness) on the biosorbent would decrease with increase in flow rate, facilitating the diffusion of metal ions through a thin film to the biosorbent. This allows film diffusion and intra-particle diffusion (IPD) to take place favorably, which results in a significant increase in the saturation concentration (N_o), as supported by the observations of the Adams-Bohart Model, where N_o values of Cr(III) and Pb(II) are increased from 858 to 3,890 mg L^{-1}, and from 5,912 to 7,041 mg L^{-1}, respectively, with increase in flow rate [4.0 to 16.0 mL min^{-1} for Cr(III) and 12.0 to 20.0 mL min^{-1} for Pb(II)]. As the effect of the increase in flow rate on sorption of metal ions and that of the increase in bed height are inversely related, an opposite

situation, as explained above, would be expected with increase in bed height. Increase in bed height would cause increase in retention time in the biosorption system, thereby increasing the film thickness of biosorbent particles. This argument is supported by experimental observations given in Table 2 and Table 3, where N_o values of Cr(III) and Pb(II) have decreased from 1,871 to 818 mg L^{-1}, and from 10,054 to 4,951 mg L^{-1}, respectively, with increase in bed height from 2.5 to 10.0 cm. Further, investigation of the removal of Pb(II) by watermelon rind under dynamic conditions indicate that the N_o values have been increased with increase in flow rate, and decreased with increase in bed height (Lakshmipathy and Sarada, 2015).

Investigation of intra-particle diffusion (IPD)

Application of the modified Weber and Morris IPD model for biosorption of Cr(III) and Pb(II) on the biosorbent selected at bed heights of 2.5, 5.0, 7.5 and 10.0 cm and at flow rates of 4.0 [for Cr(III)] and 16.0 mL min^{-1} [for Pb(II)] are shown in Figure 3 and Figure 4, respectively. These flow rates for the respective metal ions were the optimum values determined, as stated in the earlier section. Regression coefficients (R^2) of graphs for sorption of both Cr(III) and Pb(II) are close to 1.0, indicating the validity of the linear relationship between the independent and the dependent variables used in the construction of plots for all bed heights attempted.

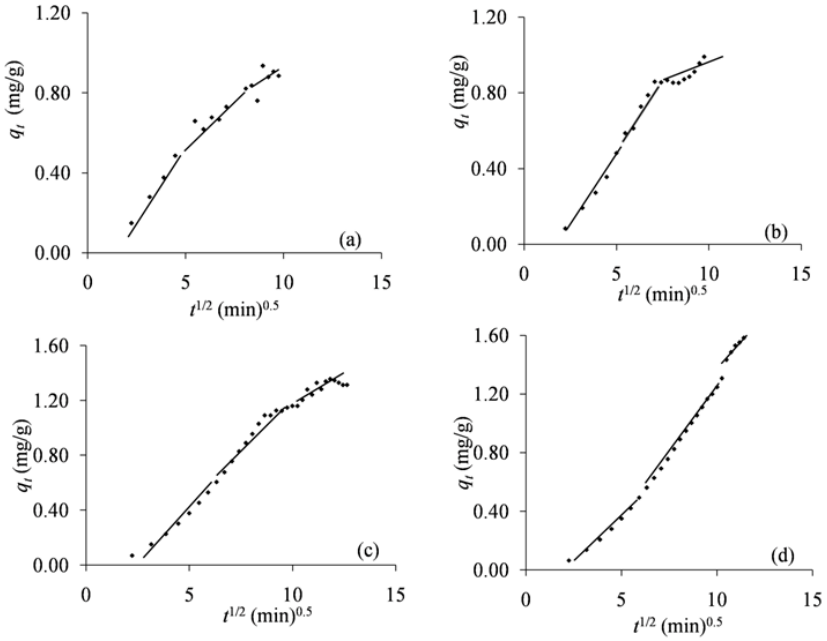

Figure 3: Variation of the amount of Cr(III) biosorbed from 10.0 mg L^{-1} solution, determined using the IPD model for the biosorbent packed in a column at a flow rate of 4.0 mL min^{-1} for different bed heights; (a) 2.5 cm, (b) 5.0 cm, (c) 7.5 cm, (d) 10.0 cm.

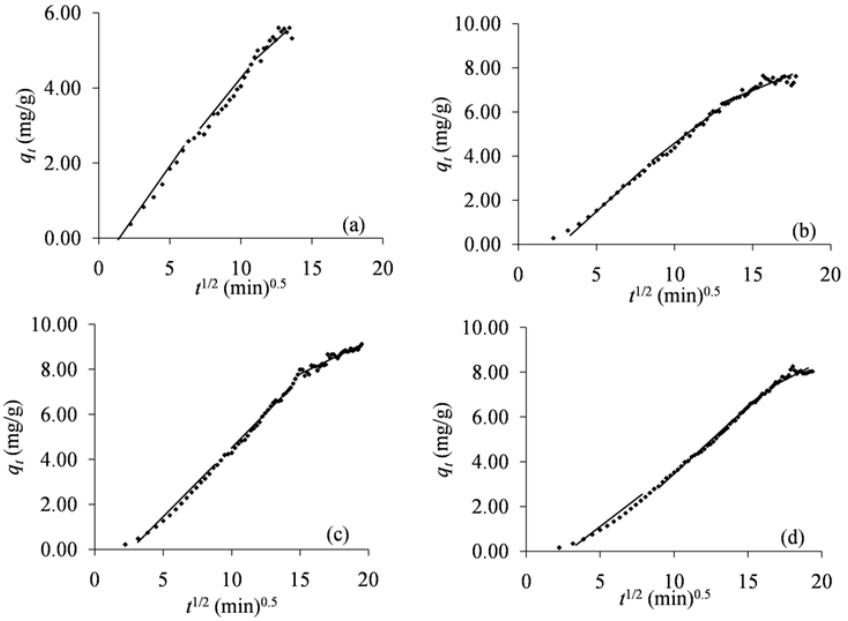

Figure 4: Variation of the amount of Pb(II) biosorbed from 10.0 mg L^{-1} solution, determined using the IPD model for the biosorbentpacked in a column at a flow rate of 16.0 mL min^{-1} for different bed heights; (a) 2.5 cm, (b) 5.0 cm, (c) 7.5 cm, (d) 10.0 cm.

According to the modified form of the Weber and Morris IPD model given in Equation (1), slopes (IPD rate constant) and intercepts (Boundary layer thickness), determined at different bed heights of the effluent solutions containing either Cr(III) or Pd(II), show the trends shown in Figure 5. Although the boundary layer thickness was initially introduced to account for the efficiency of biosorption under static conditions, it can be argued that the boundary layer be disturbed under dynamic conditions due to rapid and continuous motion of the mobile phase. It is thus reasonable to assume that boundary layer retarded IPD be expected under dynamic conditions. This is clear for biosorption of both Cr(III) and Pb(II) on the biosorbent by observing negative intercepts (Tables 4 and 5). As the extent of retardation of IPD could depend on the bed height, increase in bed height would result in more negative values of the intercept (Table 5). The observed variation of the slopes and intercepts for both Cr(III) and Pb(II) sorption provides evidence supporting this argument (Figure 5). According to the IPD model, boundary layer is developed on each and every biosorbent particle in the column. When the bed height increases gradually, the number of biosorbent particles increases simultaneously, and consequently, large number of boundary layers is overlapped creating a complex environment. Moreover, increased bed heights lead to longer retention times which then promote desorption as well. Therefore, the biosorption process is retarded more and more by the boundary layer thickness when the bed height is increased. In addition, according to Figure 5(b), zero boundary layer effect is observed for Cr(III) at a bed height of 3.0 cm and at the flow rate of 4.0 mLmin^{-1}, and therefore, higher removal efficiency for Cr(III) can be obtained using the bed column having the ratio of mass of biosorbent to flow rate at 0.900 g : 4.0 mL min^{-1}.

According to Figure 5(a), k_i values of the modified IPD Model for both Cr(III) and Pb(II) are increased at a similar rate, although the intercept is higher for Pb(II). The C values of both metal ions show that IPD rate constant has changed in each case. Therefore, it is clear that the boundary layer thickness directly affects the rate of biosorption, which can be considered as the rate limiting step. The values of C of Pb(II), in general, are more negative than those of Cr(III), revealing that the intra-particle diffusion is more retarded in the biosorption process of Pb(II). Smaller hydrated radius of Pb(II) as compared to that of Cr(III) is a possible reason for this observation. As the diffusion is the initial step of biosorption process, and as metal ions move from the solution phase to pores of different sizes on the biosorbent surface through diffusion to complete biosorption, the hydrated radius of the metal ion plays a major role in adsorption (Kotabewatta *et al*., 2020). However, detailed investigation of the behaviour of different metal ions with different biosorbents would be needed to generalize adsorption characteristics with regard to intra-particle diffusion under dynamic conditions.

Table 4: Variation of slope (k_i) and intercept (C) of IPD model with different flow rates.

Flow rate (mL min^{-1})	Cr(III)	
	k_i(mg g^{-1} min$^{-1/2}$)	C(mg g^{-1})
4.0	0.165	- 0.292
8.0	0.204	- 0.280
16.0	0.173	- 0.030
Flow rate (mL min^{-1})	**Pb(II)**	
	k_i(mg g^{-1} min$^{-1/2}$)	C(mg g^{-1})
12.0	0.665	- 2.632
16.0	0.547	- 0.917
20.0	0.627	- 0.643

Table 5: Variation of slope (k_i) and intercept (C) of IPD model with different bed heights.

Bed height (cm)	Cr(III)		Pb(II)	
	k_i (mg g^{-1} min$^{-1/2}$)	C (mg g^{-1})	k_i (mg g^{-1} min$^{-1/2}$)	C (mg g^{-1})
2.5	0.084	+ 0.133	0.416	- 0.160
5.0	0.158	- 0.290	0.581	- 1.346
7.5	0.194	- 0.620	0.648	- 2.079
10.0	0.195	- 0.688	0.564	- 2.135

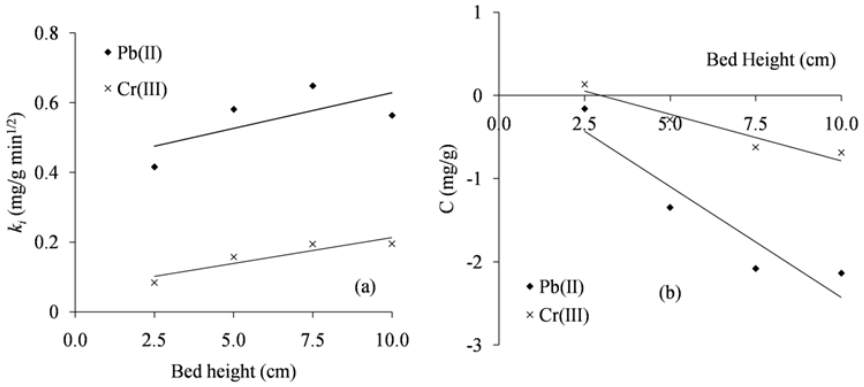

Figure 5: Variation of slope (k_i) and intercept (C) with bed heights at a flow rate of 4.0 mL min^{-1} for Cr(III) and 16.0 mL min^{-1} for Pb(II) as per the modified IPD model.

According to Equation (3), the value of R_i is related to the ratio between the initial concentration (C_i) and the final concentration (q_{ref}) of biosorption. Values of R_i and C_i/q_{ref} calculated for Cr(III) and Pb(II) for different flow rates and different bed heights are given in Table 6. According to the table, the R_i values increase from 0.76 to 0.90 [for Cr(III)], and from 0.64 to 0.89 [for Pb(II)] with increase in flow rates. On the other hand, C_i/q_{ref} values decrease from 0.24 to 0.10, and 0.36 to 0.11 for Cr(III) and Pb(II), respectively, under similar conditions. Therefore, increase in flow rate would cause changes in the initial biosorption behaviour from intermediate [Zone 2: $0.5 < R_i < 0.9$, $0.1 < C_i/q_{ref} < 0.5$] to weakly initial biosorption behaviour [Zone 1: $0.9 < R_i < 1.0$,$0 < C_i/q_{ref} < 0.1$)] (Ofomaja, 2010). Further, R_i values decrease from 0.85 to 0.59, and 0.97 to 0.73 for Cr(III) and Pb(II), respectively, with increase in bed height, while C_i/q_{ref} values increase from 0.15 to 0.41, and 0.03 to 0.27 for the same metal ions, indicating that the initial biosorption behaviour remains in intermediately initial biosorption (Zone 2) for Cr(III) and it changes from Zone 1 (weakly initial biosorption) to Zone 2 (intermediate initial biosorption) for Pb(II).

In addition, the concentration gradient (CG) may be created along the bed heights due to maintenance of different flow rates and bed heights. The CG value estimated dividing removal percentage by the respective bed height for both Cr(III) and Pb(II) under different conditions, shown in Table 6, are found to be correlated with the boundary layer thickness (C) of the IPD model. The CG and C independently show an opposite correlation with flow rate, while they show a direct correlation with bed height. Based on the findings in Table 7, it can be argued that, if CG could be increased by more than 20%, biosorption efficiency would be accelerated without boundary layer retardation.

Table 6: Variation of initial adsorption factor (R_i) and C_i/q_{ref} for different flow rates and different bed heights as per intra-particle diffusion model for Cr(III) Pb(II).

Flow rate (mL min^{-1})	Cr(III)		Flow rate (mL min^{-1})	Pb(II)	
	R_i	C_i/q_{ref}		R_i	C_i/q_{ref}
4.0	0.76	0.24	12.0	0.64	0.36
8.0	0.88	0.12	16.0	0.86	0.14
16.0	0.90	0.10	20.0	0.89	0.11
Bed height (cm)			**Bed height (cm)**		
2.5	0.85	0.15	2.5	0.97	0.03
5.0	0.71	0.29	5.0	0.82	0.18
7.5	0.54	0.46	7.5	0.77	0.23
10.0	0.59	0.41	10.0	0.73	0.27

Table 7: Concentration gradient of Cr(III)* and Pb(II)* for different bed heights.

Flow rate (mL min^{-1})	Cr(III)		Flow rate (mL min^{-1})	Pb(II)	
	Removal percentage (%)	Concentration gradient (% cm^{-1})		Removal percentage (%)	Concentration gradient (% cm^{-1})
4.0	98	9.8	12.0	78	15.6
8.0	88	8.8	16.0	72	14.4
16.0	62	6.2	20.0	70	14.0
Bed height (cm)	**Cr(III)**		**Bed height (cm)**	**Pb(II)**	
	Removal percentage (%)	Concentration gradient (% cm^{-1})		Removal percentage (%)	Concentration gradient (% cm^{-1})
2.5	50	20	2.5	42	16.8
5.0	81	16.2	5.0	72	14.4
7.5	99	13.3	7.5	90	12.0
10.0	98	9.8	10.0	90	9.0

***** Optimization of flow rate was proceeded using 10.0 cm and 5.0 cm bed heights of biosorbent for Cr(III) and Pb(II), respectively.

CONCLUSIONS

Equilibrium uptake per gram of biosorbent, q_o of the Thomas model increases with decrease in flow rate and increase in bed height for both Cr(III) and Pb(II) metal ions. Further, the saturation concentration (N_o) of the Adams–Bohart model and the time required for 50% adsorbate breakthrough (τ) of the Yoon Nelson model are important parameters to be considered in constructing packed columns to treat Cr(III) and Pb(II) ions under dynamic conditions with high efficiency. The biosorption behaviour of both metal ions is controlled by the boundary layer thickness of the biosorbent. Further, impact of flow rate and the bed height on the biosorption process indicates that intra-particle diffusion is involved in biosorption. The decrease in boundary layer thickness (C) with increase in flow rates and the increase in the C with increase in bed height were determined based on experimental data. More specifically, negative values obtained for many bed heights in contrast to positive values reported in many static conditions, indicate that the sorption of both Cr(III) and Pb(II) on the peel of *Artocarpus nobilis* fruit under dynamic condition is mainly associated with boundary layer thickness retarded intra-particle diffusion. The retardation effect becomes more significant when the bed height is increased. Detailed investigation of the behaviour of different metal ions with different biosorbents would be needed to generalize adsorption characteristics with regard to intra-particle diffusion under dynamic conditions.

Conflict of Interest: The authors declare that they have no conflict of interest.

REFERENCES

Aksu, Z. and Gönen, F. (2004). Biosorption of phenol by immobilized activated sludge in a continuous packed bed: prediction of breakthrough curves. *Process Biochemistry*, **39**(5), 599–613. https://doi.org/10.1016/S0032-9592(03)00132-8

Al-Asheh, S., Banat, F., Al-Omari, R. and Duvnjak, Z. (2000). Predictions of binary sorption isotherms for the sorption of heavy metals by pine bark using single isotherm data. *Chemosphere*, **41**(5), 659–665. https://doi.org/10.1016/S0045-6535(99)00497-X

Albadarin, A. B., Al-muhtaseb, A. H., Al-laqtah, N. A., Walker, G. M., Allen, S. J. and Ahmad, M. N. M. (2011). Biosorption of toxic chromium from aqueous phase by lignin : mechanism , effect of other metal ions and salts. *Chemical Engineering Journal*, **169**(1–3), 20–30. https://doi.org/10.1016/j.cej.2011.02.044

Ali, R. M., Hamad, H. A., Hussein, M. M. and Malash, G. F. (2016). Potential of using green adsorbent of heavy metal removal from aqueous solutions: Adsorption kinetics, isotherm, thermodynamic, mechanism and economic analysis. *Ecological Engineering*, **91**, 317–332. https://doi.org/10.1016/j.ecoleng.2016.03.015

Aljeboree, A. M., Alshirifi, A. N. and Alkaim, A. F. (2017). Kinetics and equilibrium study for the adsorption of textile dyes on coconut shell activated carbon. *Arabian Journal of Chemistry*, **10**, S3381–S3393. https://doi.org/10.1016/j.arabjc.2014.01.020

Biswas, S. and Mishra, U. (2015). Continuous fixed-bed column study and adsorption modeling: Removal of lead ion from aqueous solution by charcoal originated from chemical carbonization of rubber wood sawdust. *Journal of Chemistry*, **2015**, 1–9. https://doi.org/10.1155/2015/907379

Calero, M., Hernáinz, F., Blázquez, G., Tenorio, G. and Martín-Lara, M. A. (2009). Study of Cr (III) biosorption in a fixed-bed column. *Journal of Hazardous Materials*, **171**(1–3), 886–893. https://doi.org/10.1016/j.jhazmat.2009.06.082

Chatterjee, S., Mondal, S. and De, S. (2018). Design and scaling up of fixed bed adsorption columns for lead removal by treated laterite. *Journal of Cleaner Production*, **177**, 760–774. https://doi.org/10.1016/j.jclepro.2017.12.249

Chieng, H. I., Lim, L. B. L. and Priyantha, N. (2015). Sorption characteristics of peat from Brunei Darussalam for the removal of rhodamine B dye from aqueous solution: adsorption isotherms, thermodynamics, kinetics and regeneration studies. *Desalination and Water Treatment*, **55**(3), 664–677. https://doi.org/10.1080/19443994.2014.919609

Crittenden, J. C., Hutzler, N. J., Geyer, D. G., Oravitz, J. L. and Friedman, G. (1986). Transport of organic compounds with saturated groundwater flow: Model development and parameter sensitivity. *Water Resources Research*, **22**(3), 271–284. https://doi.org/10.1029/WR022i003p00271

Farooq, U., Athar, M., Khan, M. A. and Kozinski, J. A. (2013). Biosorption of Pb(II) and Cr(III) from aqueous solutions: breakthrough curves and modeling studies. *Environmental Monitoring and Assessment*, **185**(1), 845–854. https://doi.org/10.1007/s10661-012-2595-z

Foo, K. Y. and Hameed, B. H. (2010). Insights into the modeling of adsorption isotherm systems. *Chemical Engineering Journal*, **156**(1), 2–10. https://doi.org/10.1016/j.cej.2009.09.013

Gerente, C., Lee, V. K. C., Cloirec, P. Le and McKay, G. (2007). Application of chitosan for the removal of metals from wastewaters by adsorption—Mechanisms and models review. *Critical Reviews in Environmental Science and Technology*, **37**(1), 41–127. https://doi.org/10.1080/10643380600729089

Girish, C. R. and Murty, V. R. (2016). Mass transfer studies on adsorption of Phenol from wastewater using *Lantana camara* , Forest waste. *International Journal of Chemical Engineering*, **2016**, 1–11. https://doi.org/10.1155/2016/5809505

Gutiérrez-Segura, E., Solache-Ríos, M., Colín-Cruz, A. and Fall, C. (2014). Comparison of cadmium adsorption by inorganic adsorbents in column systems. *Water, Air and Soil Pollution*, **225**(6), 1943. https://doi.org/10.1007/s11270-014-1943-8

Han, R., Wang, Y., Zhao, X., Wang, Y., Xie, F., Cheng, J. and Tang, M. (2009). Adsorption of methylene blue by phoenix tree leaf powder in a fixed-bed column: Experiments and prediction of breakthrough curves. *Desalination*, **245**(1–3), 284–297. https://doi.org/10.1016/j.desal.2008.07.013

Hasan, S. H., Ranjan, D. and Talat, M. (2010). Agro-industrial waste 'wheat bran' for the biosorptive remediation of selenium through continuous up-flow fixed-bed column. *Journal of Hazardous Materials*, **181**(1–3), 1134–1142. https://doi.org/10.1016/j.jhazmat.2010.05.133

Jagtap, U. B. and Bapat, V. A. (2010). Artocarpus: A review of its traditional uses, phytochemistry and pharmacology. *Journal of Ethnopharmacology*, **129**(2), 142–166. https://doi.org/10.1016/j.jep.2010.03.031

Kotabewatta, P. A., Priyantha, N. and Lim, L. B. L. (2020). Biosorption of heavy metal ions on peel of *Artocarpus nobilis* fruit: 2. Improvement of biosorption capacities of Ni(II) through different modifications. *Desalination and Water Treatment*, **185**, 226–236. https://doi.org/10.5004/dwt.2020.25412

Kumar, S., Patra, C., Narayanasamy, S. and Rajaraman, P. V. (2020). Performance of acid-activated water caltrop (*Trapa natans*) shell in fixed bed column for hexavalent chromium removal from simulated wastewater. *Environmental Science and Pollution Research*, **27**(22), 28042–28052. https://doi.org/10.1007/s11356-020-09155-8

Lakshmipathy, R. and Sarada, N. C. (2015). A fixed bed column study for the removal of Pb^{2+} ions by watermelon rind. *Environmental Science: Water Research and Technology*, **1**(2), 244–250. https://doi.org/10.1039/C4EW00027G

Lim, A. P. and Aris, A. Z. (2014). Continuous fixed-bed column study and adsorption modeling: Removal of cadmium (II) and lead (II) ions in aqueous solution by dead calcareous skeletons. *Biochemical Engineering Journal*, **87**(May), 50–61. https://doi.org/10.1016/j.bej.2014.03.019

Lim, L. B. L., Priyantha, N., Hei Ing, C., Khairud Dahri, M., Tennakoon, D. T. B., Zehra, T. and Suklueng, M. (2013). *Artocarpus odoratissimus* skin as a potential low-cost biosorbent for the removal of methylene blue and methyl violet 2B. *Desalination and Water Treatment*, **73**(7), 3239–3247. https://doi.org/10.1080/19443994.2013.852136

Lim, L. B. L., Priyantha, N. and Mansor, N. H. M. (2015). *Artocarpus altilis* (breadfruit) skin as a potential low-cost biosorbent for the removal of crystal violet dye: equilibrium, thermodynamics and kinetics studies. *Environmental Earth Sciences*, **73**(7), 3239–3247. https://doi.org/10.1007/s12665-014-3616-8

Long, Y., Lei, D., Ni, J., Ren, Z., Chen, C. and Xu, H. (2014). Packed bed column studies on lead(II) removal from industrial wastewater by modified *Agaricus bisporus*. *Bioresource Technology*, **152**, 457–463. https://doi.org/10.1016/j.biortech.2013.11.039

Malkoc, E., Nuhoglu, Y. and Abali, Y. (2006). Cr(VI) adsorption by waste acorn of *Quercus ithaburensis* in fixed beds: Prediction of breakthrough curves. *Chemical Engineering Journal*, **119**(1), 61–68. https://doi.org/10.1016/j.cej.2006.01.019

Marzbali, M. H. and Esmaieli, M. (2017). Fixed bed adsorption of tetracycline on a mesoporous activated carbon: Experimental study and neuro-fuzzy modeling. *Journal of Applied Research and Technology*, **15**(5), 454–463. https://doi.org/10.1016/j.jart.2017.05.003

Mckay, G. (2007). The adsorption of dyestuffs from aqueous solutions using activated carbon. iii. intraparticle diffusion processes. *Journal of Chemical Technology and Biotechnology. Chemical Technology*, **33**(4), 196–204. https://doi.org/10.1002/jctb.504330406

Mitra, T., Singha, B., Bar, N. and Das, S. K. (2014). Removal of Pb(II) ions from aqueous solution using water hyacinth root by fixed-bed column and ANN modeling. *Journal of Hazardous Materials*, **273**(Ii), 94–103. https://doi.org/10.1016/j.jhazmat.2014.03.025

Ofomaja, A. E. (2010). Intraparticle diffusion process for lead(II) biosorption onto mansonia wood sawdust. *Bioresource Technology*, **101**(15), 5868–5876. https://doi.org/10.1016/j.biortech.2010.03.033

Özcan, A. S. and Özcan, A. (2004). Adsorption of acid dyes from aqueous solutions onto acid-activated bentonite. *Journal of Colloid and Interface Science*, **276**(1), 39–46. https://doi.org/10.1016/j.jcis.2004.03.043

Priyantha, N. and Kotabewatta, P. A. (2019). Biosorption of heavy metal ions on peel of *Artocarpus nobilis* fruit: 1—Ni(II) sorption under static and dynamic conditions. *Applied Water Science*, **9**(2), 37. https://doi.org/10.1007/s13201-019-0911-2

Priyantha, N., Lim, L. B. L., Tennakoon, D. T. B., Liaw, E. T. Z., Ing, C. H. and Liyandeniya, A. B. (2018). Biosorption of cationic dyes on breadfruit (*Artocarpus altilis*) peel and core. *Applied Water Science*, **8**(1), 37. https://doi.org/10.1007/s13201-018-0648-3

Saadi, Z., Saadi, R. and Fazaeli, R. (2013). Fixed-bed adsorption dynamics of Pb (II) adsorption from aqueous solution using nanostructured γ-alumina. *Journal of Nanostructure in Chemistry*, **3**(1), 48. https://doi.org/10.1186/2193-8865-3-48

Santhi, T. and Manonmani, S. (2011). Malachite green removal from aqueous solution by the peel of *Cucumis sativa* Fruit. *CLEAN - Soil, Air, Water*, **39**(2), 162–170. https://doi.org/10.1002/clen.201000077

Shahbazi, A., Younesi, H. and Badiei, A. (2011). Functionalized SBA-15 mesoporous silica by melamine-based dendrimer amines for adsorptive characteristics of Pb(II), Cu(II) and Cd(II) heavy metal ions in batch and fixed bed column. *Chemical Engineering Journal*, **168**(2), 505–518. https://doi.org/10.1016/j.cej.2010.11.053

Sheela, T. and Nayaka, Y. A. (2012). Kinetics and thermodynamics of cadmium and lead ions adsorption on NiO nanoparticles. *Chemical Engineering Journal*, **191**, 123–131. https://doi.org/10.1016/j.cej.2012.02.080

Ting, T. M., Nasef, M. M. and Hashim, K. (2016). Evaluation of boron adsorption on new radiation grafted fibrous adsorbent containing N-methyl-D-glucamine. *Journal of Chemical Technology and Biotechnology*, **91**(7), 2009–2017. https://doi.org/10.1002/jctb.4793

Wang, W., Li, M. and Zeng, Q. (2015). Adsorption of chromium (VI) by strong alkaline anion exchange fiber in a fixed-bed column : Experiments and models fitting and evaluating. *Separation And Purification Technology*, **149**(5), 16–23. https://doi.org/10.1016/j.seppur.2015.05.022

Wu, F., Tseng, R. and Juang, R. (2009). Initial behavior of intraparticle diffusion model used in the description of adsorption kinetics. *Chemical Engineering Journal*, **153**(1–3), 1–8. https://doi.org/10.1016/j.cej.2009.04.042

Xu, Z., Cai, J. and Pan, B. (2013). Mathematically modeling fixed-bed adsorption in aqueous systems. *Journal of Zhejiang University Science A*, **14**(3), 155–176. https://doi.org/10.1631/jzus.A1300029

Yan, C., Li, G., Xue, P., Wei, Q. and Li, Q. (2010). Competitive effect of Cu(II) and Zn(II) on the biosorption of lead(II) by *Myriophyllum spicatum*. *Journal of Hazardous Materials*, **179**(1–3), 721–728. https://doi.org/10.1016/j.jhazmat.2010.03.061

Zheng, W., An, Q., Lei, Z., Xiao, Z., Zhai, S., and Liu, Q. (2016). Efficient batch and column removal of Cr(VI) by carbon beads with developed nano-network. *RSC Advances*, **6**(106), 104897–104910. https://doi.org/10.1039/C6RA14070J

Zhou, Q., Gong, W., Xie, C., Yuan, X., Li, Y., Bai, C., Chen, S. and Xu, N. (2011). Biosorption of Methylene Blue from aqueous solution on spent cottonseed hull substrate for *Pleurotus ostreatus* cultivation. *Desalination and Water Treatment*, **29**(1–3), 317–325. https://doi.org/10.5004/dwt.2011.2238